Analytica Chimica Acta 1214 (2022) 339961

Contents lists available at ScienceDirect

Analytica Chimica Acta

journal homepage: www.elsevier.com/locate/aca

Ti_3C_2@WSe_2 as photoelectractive materials coupling with recombinase polymerase amplification for nucleic acid detection

Xiaohua Li [a], Ruhao Wang [b], Lizhen Liu [a], Xu Hun [b,*]

[a] College of Chemistry and Chemical Engineering, Shanxi Datong University, Datong, 037009, Shanxi, China
[b] Key Laboratory of Optic-electric Sensing and Analytical Chemistry for Life Science, MOE, Shandong Key Laboratory of Biochemical Analysis, Key Laboratory of Analytical Chemistry for Life Science in Universities of Shandong, College of Chemistry and Molecular Engineering, Qingdao University of Science and Technology, Qingdao, 266042, China

HIGHLIGHTS

- A novel material, Ti_3C_2@WSe_2, was firstly synthesized.
- A new double-redox cycling system, TCEP/SQA/4-AP, was discovered.
- SQA, 4-AP cycling played a key role in enhancing PEC signals.
- A PEC assay coupled with RPA for RSV detection with LOD 30 aM.

GRAPHICAL ABSTRACT

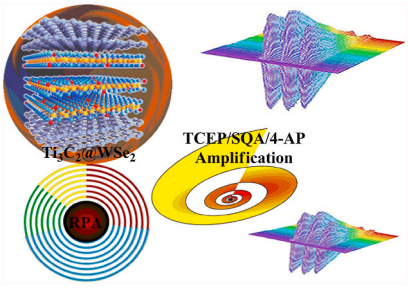

ARTICLE INFO

Keywords:
Double redox cycle
Signal amplification
Respiratory syncytial virus
WSe_2
Ti_3C_2

ABSTRACT

The photoelectrochemical biosensor based on double redox cycle amplification technology coupled with Tungsten diselenide and MXene-modified electrode was developed. Signal amplification technology is a commonly used method to improve the sensitivity. In this article, in the double redox cycle amplification method, *p*-aminophenol is used as the signal molecule, and squaric acid acts as a redox indicator. Tris(2-carboxyethyl) phosphine is an excellent reducing agent, which greatly improves the photoelectric response. Tungsten diselenide and MXene are used as photosensitive materials. In the presence of model target, respiratory syncytial virus RNA, the recombinase polymerase amplification process occurred because there is amplification template, so that the signal molecule *p*-aminophenol will be produced, leading to redox cycle was carried out, and the photocurrent signal is improved. In the absence of syncytial virus RNA, the photocurrent signal is low. The detection range of the biosensor is from 0.2 fM to 80 fM, and the detection limit reaches 30 aM for respiratory syncytial virus RNA. The method of introducing redox cycle amplification and Tungsten diselenide, MXene into photoelectrochemical biosensing provides a new idea for future biological analysis and has application potential.

* Corresponding author.
E-mail address: hunxuprof@outlook.com (X. Hun).

https://doi.org/10.1016/j.aca.2022.339961
Received 29 March 2022; Received in revised form 16 May 2022; Accepted 17 May 2022
Available online 21 May 2022

1. Introduction

As we all know, a mushrooming number of 2D materials with large surface areas are used as matrix materials for nano-precious metals to improve the conduction, biocompatibility and catalytic performance of nano-composite materials [1]. In recent years, titanium carbide Mxene, a member of two-dimensional layered nanomaterials, has gradually attracted people's attention [2]. It has a large surface area of nano-structure, excellent electron transfer ability, catalytic ability and biocompatibility, etc. [3,4] The unique properties of the nanomaterial make it has the potential for applications in biosensing. Among a variety of photosensitive materials, transition metal disulfides analogues with a layered structure are also expected to be highly anticipated due to their excellent mechanical, physical and chemical properties. Especially the stable semiconductor material tungsten diselenide, which has the advantages of tunable band gap, high carrier mobility and small size, especially under light conditions, shows excellent performance, therefore, tungsten diselenide (WSe_2) is also a very promising sensing material [5]. Due to the electrical conductivity of the core transition metal in the layered structure, Ti_3C_2 exhibit considerable electron density near Fermi level. High conductivity helps ensure fast transport of electrons. In addition, Ti_3C_2 can form a Schottky barrier with semiconductors by virtue of the lower Fermi energy level relative to the conduction band of semiconductors to facilitate high-speed electron transport and facilitate the separation of photogenerated electron-hole pairs [6]. Therefore, compounding Ti_3C_2 to WSe_2 enables the effective improvement of photoelectric conversion efficiency.

On the other hand, many researchers of photoelectrochemical (PEC) biosensors have studied the factors that influence the increase or decrease of PEC signal, and there are many studies on electron donors or electron acceptors [7,8]. A large number of studies have shown that electron donors or electron acceptors are an important way to improve the sensitivity of PEC. The most common small molecules are dopamine, ascorbic acid, *p*-aminophenol, ferrocene formic acid, ferrocyanide, methionine, and so on [9–11]. In addition, the effects of active substances in redox cycle amplification [12] and dual redox cycle amplification [13] on PEC signals have also been studied. The dual redox reaction has obvious advantages due to its higher electron transfer number and higher electron-hole separation efficiency during the reaction. Combinatorial using of multiple small molecules lays the foundation for enhanced photocurrent.

Here, we found that the interaction between photoactive materials and small molecules will greatly promote the photocurrent. We have developed a strategy based on double redox cycle amplification technology combined with in situ recombinase polymerase amplification (RPA) to detect nucleic acid. The respiratory syncytial virus nucleic acid was used as model target. Respiratory syncytial virus is a kind of Pneumovirus genus of Paraviridae family, and is crucial viral pathogens that cause respiratory infections in children and the elderly. It is an RNA virus that is transmitted by air droplets and close contact. The incubation period is three to seven days. Respiratory syncytial virus infection causes clinical manifestations, such as otitis media, mild upper respiratory tract infections, and potentially fatal lower respiratory tracts [14]. So far, the commercial vaccine is lack. Ribavirin and Palivizumab are the alternative for the treatment of retroviral infections, but researches have shown that they are not completely effective [15]. Therefore, a convenient and sensitive diagnostic method is essential for the clinical diagnosis of respiratory syncytial virus infection.

First, we modify the carbon paste electrode (CPE) with flake titanium carbide (Ti_3C_2) and tungsten diselenide (WSe_2) (Ti_3C_2@WSe_2), and then drop the dispersion of gold nanoparticles on the material modified electrode. After the film is formed, the formed electrode is modified with forward primer with the interaction of gold-sulfur bond. Respiratory syncytial virus (RSV) is selected as the model target used as a template for reverse transcription and then amplified in situ by RPA. The product of RPA binds to streptavidin alkaline phosphatase (SA-ALP). ALP catalyzes the hydrolysis reaction of *p*-aminophenyl phosphate monosodium (4-APP) to generate the electron donor *p*-aminophenol (4-AP). Due to the redox effect of 4-AP and squaric acid (SQA) and dicarboxyethyl phosphate (TCEP), the electrons continue to increase, which in turn increases the PEC signal. As the RSV concentration increases, more SA-ALPs are connected to the electrodes. Enzyme catalysis based on ALP enhances the photocurrent response through the continuous generation of electrons. Based on the strategy of RPA and dual redox cycle amplification technology, the relationship between photocurrent and RSV concentration was developed, and this PEC biosensor has the characteristics of high sensitivity, good selectivity, and broad application prospects.

2. Experimental section

2.1. Reagents and apparatus

Bulk tungsten diselenide (WSe_2) was purchased from J&K Scientific Ltd. (Beijing, China). Ti_3AlC_2 was obtained from Sciclubs (Zhejiang, China). 4-aminophenylphosphate monosodium (4-APP) was obtained from Biosynth Carbosynth (United Kingdom). Strepavidin-alkaline phosphatase (SA-ALP), 4-aminophenol (4-AP), Squaric acid (SQA) and Tris(2-carboxyethyl)phosphine (TCEP) and all the other reagents were purched from ABCR (Karlsruhe, Germany). DNA were synthesized by Sangon Biotech (Shanghai, China) (SH-ATACACTATTCAACGTAGTA-CAGGAGA, SH-FP; Biotin-TGAATTTATGATTTGCATCTTCAGTGATT, Biotin-RP).

The morphology of WSe_2, Ti_3C_2, WSe_2/Ti_3C_2 and AuNPs were characterizated by TEM (JEM-2100, USA). The others information of reagents and apparatus provided in Supporting Information **S1** and **S2**.

2.2. Preparation of WSe_2/Ti_3C_2 and AuNPs

First, 2 g Ti_3AlC_2 and 2 g LiF were accurately weighed. Then 40 mL HCl (9 M) was measured with plastic measuring cylinder and slowly transferred into the Teflon beaker. Then LiF was added to the beaker and stirred for 30 min. After stirring, Ti_3AlC_2 was added in a slow process. Then magnetic stirring was carried out at room temperature for 24 h at 200 rpm. After stirring, the solution was centrifuged at 4000 rpm for cleaning. Centrifugation was stopped until the pH of upper turbid solution reaches 6. The Ti_3C_2 was obtained. Finally, the precipitate was dried in vacuum and stored at 4 °C. Then 0.0120 g Ti_3C_2 and 0.0120 g bulk WSe_2 were dispersed in DMF respectively. The WSe_2 solution was ultrasoniced for 4 h, and thin sheet WSe_2 were obtained. Finally, 2 mL Ti_3C_2 and WSe_2 dispersions were mixtured evenly. WSe_2/Ti_3C_2 were gained.

0.5 mL of 100 mmol/L $HAuCl_4{\cdot}4H_2O$ and 0.5 mL of 100 mmol/L sodium citrate were added sequentially to 18 mL ultra pure water at room temperature and stirred for 5 min. Then 0.85 mL of 0.1 mmol/L sodium borohydride was added quickly to the mixture. The reaction was executed continuously. The basis for obtaining gold nanoparticles with a particle size of 10 nm is that the color of the solution changes from orange to orange-red.

2.3. Fabrication of PEC biosensor

15 μL WSe_2/Ti_3C_2 solution was dripped onto the fresh bare CPE surface. And it was dried naturally in the air. Then 15 μL AuNPs were modified on the electrode surface and dried.

3 μL forward primers (5 μM) were dropped onto modified electrode surfaces. Then, 5 μL MCH (0.3 mM) was added into the electrode to block the non-specific active sites of the electrode.

RPA solutions, 2.4 μL of reverse primer (10 μM), 29.5 μL of rehydration buffer and 13.2 μL of Dnase-free water, were mixed. Then they were added to the freeze-dried enzyme pellet. The mixture and magnesium acetate at a concentration of 280 mM (2.5 μL) were added to the

tube. 10 μL RSV then was added. The reaction volume of 15 μL was added onto AuNPs/WSe_2/Ti_3C_2/CPE. It was reacted at 37 °C for 30 min.

3. Results and discussion

3.1. Morphological characterization of nanomaterials

The morphology of WSe_2 was characterized by TEM. As shown in Fig. 1A, the WSe_2 exhibits irregular hexagonal shapes, and after exfoliation, the WSe_2 became thinner and smaller. The Ti_3AlC_2 exhibits a massive morphology with a smooth surface (Fig. 1B). And the lateral of Ti_3AlC_2 is shown in Fig. 1B insert, but the layered structure is not obvious. After HF etching Al layers, the bulk Ti_3AlC_2 is transformed into the typical organ like structure. This appearance indicates that the Ti_3C_2 is successfully prepared (Fig. 1C) [16,17]. Elemental mapping results of Fig. 1E show that elements of C, Ti, Se and W were well-distributed. And that further confirming the formation of the WSe_2/Ti_3C_2 (Fig. 1D) [18]. The morphologies of bulk WSe_2 and AuNPs were characterized by TEM were provided in **S3**.

Fig. 1F shows the XRD patterns of the WSe_2, Ti_3C_2 and WSe_2/Ti_3C_2. For the Ti_3C_2 or WSe_2/Ti_3C_2, the only strong diffraction peak is located at around $2\theta = 8.98^o$, which matches well with literature reports about Ti_3C_2 Mxene [19]. After etching Ti_3AlC_2 with HF treatment, it is hard to observe the characteristic peak at around 40^o of Ti_3C_2 or WSe_2/Ti_3C_2 [20,21]. This phenomenon shows that the Al layers had successfully fallen off and the appearance of multilayered Ti_3C_2 according to reference. [22] The intensity of the peaks were weakened after Ti_3C_2 complex loading, which may be due to the Ti_3C_2 complex loaded on the surface of WSe_2 influencing the detection of the WSe_2 substrate by X-ray. The WSe_2/Ti_3C_2 composite exhibited combinatorial XRD spectra of pure WSe_2 and Ti_3C_2.

3.2. PEC property of the AuNPs/WSe_2/Ti_3C_2

Here, the basic properties of the sensor were investigated through the modified electrode. The process was detected in the phosphate buffer. WSe_2 photocurrent response is 111.4 nA (Fig. 2A), and Ti_3C_2 photocurrent response is 211.1 nA. But when WSe_2 and Ti_3C_2 were combined together, the photocurrent response is greatly enhanced (425.6 nA). The addition of AuNPs improves the photocurrent response slightly (512.7 nA). It might be that AuNPs increases the conductivity of the electrode. The photocurrent response of the AuNPs/WSe_2/Ti_3C_2/CPE in phosphate buffer contained different molecules was then evaluated as depicted in Fig. 2B. The photocurrent response of TCEP, SQA, 4-AP are 1510.2 nA, 1644.5 nA and 2242.7 nA, respectively. It can be seen that those molecules could enhance the photocurrent response. The three substances could be easy oxidized by the photogenerated holes of the photoelectrode and depressed the electron-hole pair recombination. For the TCEP/SQA system, there was no significant difference from the photocurrent response of TCEP or SQA alone. For the TCEP/4-AP system, its response was much higher than that of TCEP or 4-AP because of the 4-AP regeneration from the 4-quinone imine (4-QI) [23]. And the photocurrent response was 3155.0 nA. Similarly, signal enhancement of SQA/4-AP was caused by the regeneration of CBO from the reaction between SQA, CBT and 4-AP. And the photocurrent response reached 2882.2 nA. However, the highest photocurrent (11180.9 nA) was observed in the TCEP/SQA/4-AP system. These results clearly demonstrated that the coexistence of TCEP, SQA and 4-AP had a particularly good response to the WSe_2/Ti_3C_2/AuNPs/CPE. And the TCEP/SQA/4-AP system had great potential for increasing the sensitivity of the bioanalysis.

3.3. The mechanism of photocurrent generation

According to the literature, the photoinduced electrons and holes were efficiently by the light illumination [24], which occurred simultaneously in WSe_2/Ti_3C_2 composites. Hence, the band gap of WSe_2 and WSe_2/Ti_3C_2 were measured by via ultraviolet–visible diffusion reflectance spectra (UV–vis DRS). Single layer WSe_2 belongs to direct semiconductor. In addition, WSe_2/Ti_3C_2 is also classified as a direct semiconductor [25,26]. As shown in Fig. 3 A, B, the band gap of WSe_2 is 1.30 eV and that of WSe_2/Ti_3C_2 is 1.20 eV. The shortened band gap of WSe_2 is attributed to the addition of Ti_3C_2. As illustrated in Fig. 2B, under the condition of light irradiation, the photocurrent response of the WSe_2/Ti_3C_2/CPE is significantly higher than that of WSe_2. The existence of Ti_3C_2 not only narrowed the band gap of WSe_2 but also enhanced its light absorption ability [27,28].

According to the Mott-Schottky measurements, the type of semiconductor can be determined by tangent to the longest straight line of the curve. As shown in Fig. 3C, the slopes of the tangents were positive, which illustrated that the samples are n-type semiconductors. And the flat band potential (E_{FB}) can be inferred from the intersection of the epitaxial tangent and the abscissa. Thus, the E_{FB} of WSe_2 and Ti_3C_2 were around – 0.5 eV and – 0.25 eV, respectively. Based on the published

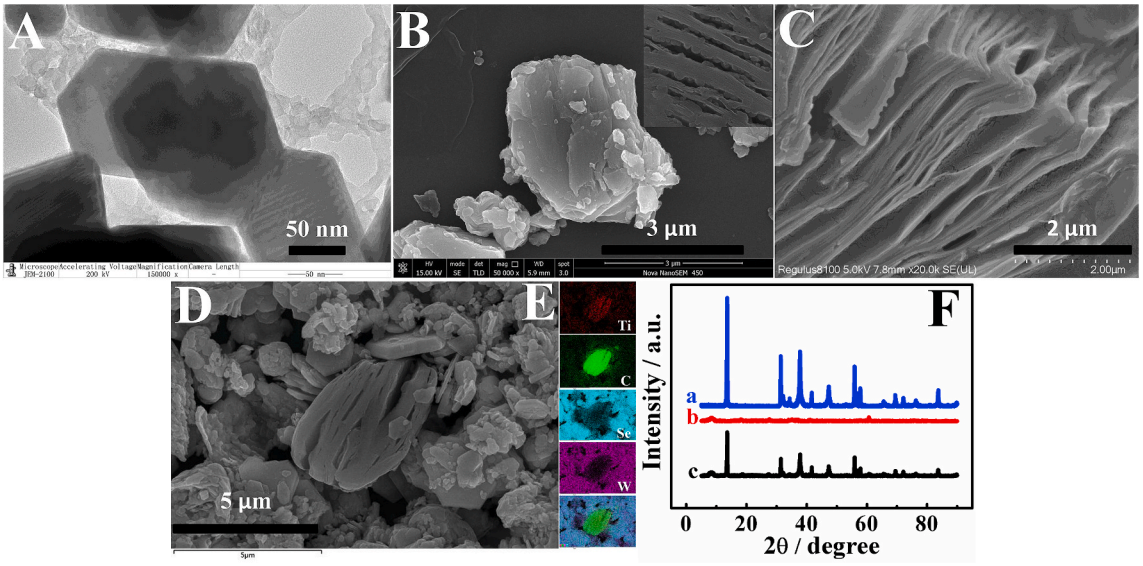

Fig. 1. TEM images of WSe_2 **(A)**. SEM images of Ti_3AlC_2 **(B)**, Ti_3C_2 **(C)** and WSe_2/Ti_3C_2 **(D)**. Elemental mapping of WSe_2/Ti_3C_2 **(E)**. **(F)** XRD patterns of WSe_2 **(a)**, Ti_3C_2 **(b)** and WSe_2/Ti_3C_2 **(c)**. The insert in **(B)** is the side view of Ti_3AlC_2.

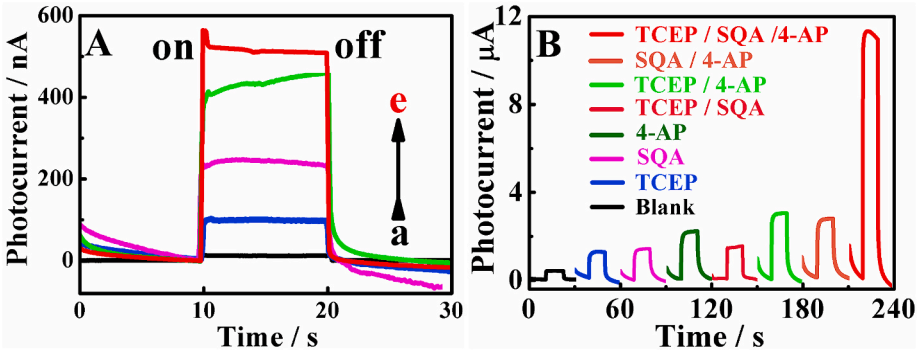

Fig. 2. **(A)** The photocurrent response of CPE, WSe_2, Ti_3C_2, WSe_2/Ti_3C_2, AuNPs/WSe_2/Ti_3C_2 in phosphate buffer (the peak from a to e). **(B)** The photocurrent response of AuNPs/WSe_2/Ti_3C_2 in phosphate buffer contained different small molecules.

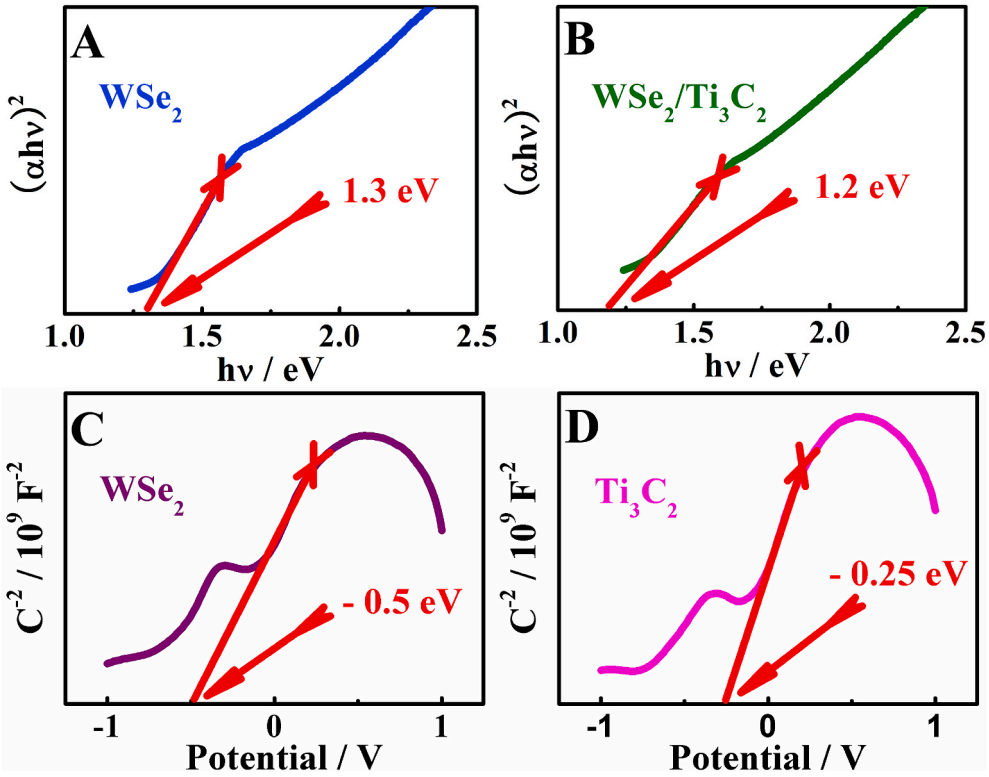

Fig. 3. UV–vis DRS of WSe_2 **(A)** and WSe_2/Ti_3C_2 **(B)**. Mott-Schottky of WSe_2 **(C)** and Ti_3C_2 **(D)**.

reports, for n-type semiconductors, the E_{FB} is about 0.1 eV higher than the CB. The CB edge of WSe_2 is −0.4 eV. The minimum value of VB can be calculated according to equation (1). Based on the above investigation, the energy level structure diagram was obtained (Fig. 4).

$$E_{VB} = E_g - E_{CB} \quad (1)$$

3.4. Test and verify of redox cycle process

As shown in Fig. 5, the feasibility of the proposed PEC RPA strategy was first investigated by the cyclic voltammogram (CV) behaviors of the AuNPs/WSe_2/Ti_3C_2/CPE in different buffer solutions. There was no obvious redox peak of SQA or TCEP. The 4-AP oxidation peak appeared at 0.1 V. There was no obvious signal change in the SQA/TCEP system when the TCEP added to the SQA solution. This clearly indicated that the 4-AP was more easily oxidized than SQA. The added SQA was reduced to cyclobutaneoctol (CBO) by TCEP [13]. And then the CBO was oxidized

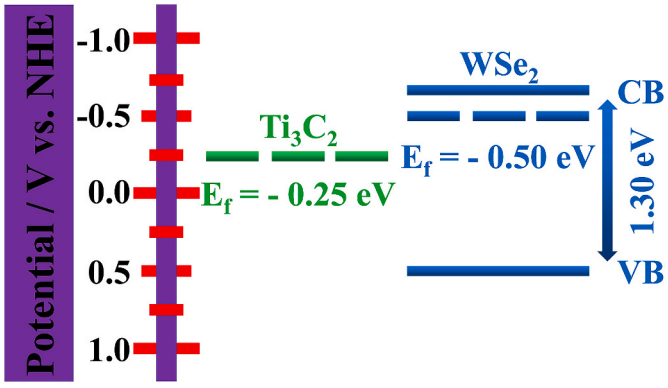

Fig. 4. Band structures of WSe_2 and Ti_3C_2.

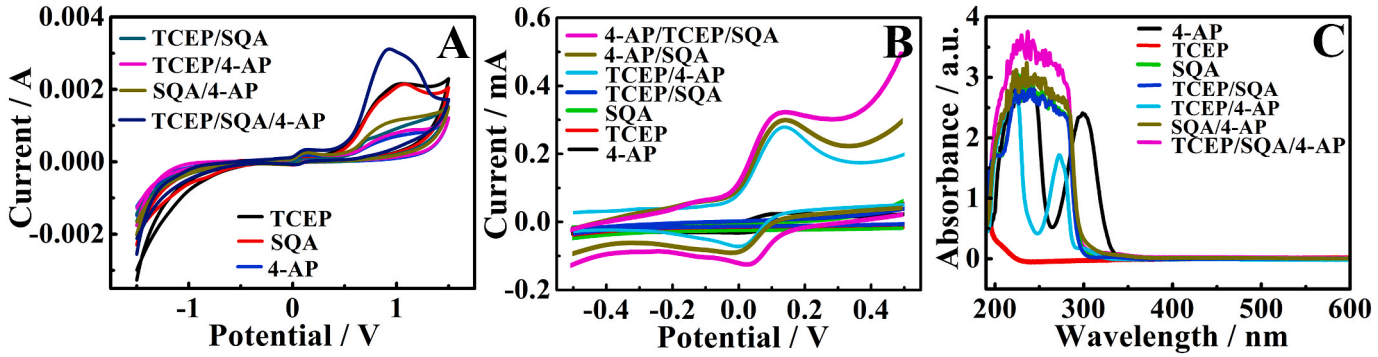

Fig. 5. **(A)** CV of AuNPs/WSe_2/Ti_3C_2 in phosphate buffer contained different small molecules. **(B)** The local graph of **(A)** at −0.5 V–0.5 V. **(C)** UV–vis of 4-AP, TCEP, SQA, TCEP/SQA, TCEP/4-AP, SQA/4-AP, TCEP/SQA/4-AP respectively.

to cyclobutanetetrone (CBT) by 4-AP. The resulting CBT was reduced again back to CBO by TCEP. Significantly, in the 4-AP/SQA/TCEP system, the peak current further increased compared to that of 4-AP/TCEP and 4-AP/SQA. It shows that the interaction between the three small molecules promoted the electron transfer, thereby resulting in the amplification of the signal.

In addition, the conversion between small molecules was explained by UV–vis spectra (Fig. 5C). The TCEP alone had no absorption peak. When 4-AP was detected separately, a distinct spectral profile with absorption at 240 nm and 300 nm were obtained. When the TCEP was added to the 4-AP, two new absorption peaks at 210 nm and 270 nm appeared. Meanwhile the peak value of 4-AP had a blue shift. There was a wider absorption peak in the system containing SQA. When 4-AP or TCEP were added to SQA solution, the peak value increased. Especially, when the three small molecules were mixed, the peak enhancement effect was the best. Thus, through the interaction of the three kinds of small molecules, the photoelectric signal can be amplified, and then the purpose of detection can be achieved.

Herein, a new sensing mechanism for enhancing photocurrent response was proposed by the arrangement of AuNPs/WSe_2/Ti_3C_2 levels. As displayed in Scheme 1, upon light illumination, the electron-hole pairs of WSe_2 were separated. According to the UV–vis DRS (Fig. 3), the mixing of Ti_3C_2 narrowed the band gap and enhances the ability of WSe_2 to absorb visible light (Fig. S2). In order to suppress the recombination of electron-holes, a continuous supply of electrons was needed. In phosphate buffer solution, which containing SQA and TCEP, the SQA was reduced to CBO by TCEP. Then the generated CBO was oxidized step by step to CBT by 4-AP. And the resulting CBT was reduced again back to CBO by TCEP. This catalytic cycle allowed electrons to be continuously supplied to the solution, thereby resulting in the amplification of the photocurrent response. AuNPs absorb visible light and can transfer the electrons to the CB of the WSe_2. Moreover, the E_f of Ti_3C_2 was lower than the CB of WSe_2, which was more convenient for electron transfer. Finally, electrons were transferred to the CPE surface to achieve the purpose of detection.

3.5. Characterization of the PEC biosensor fabrication

The principle of RSV detection was shown in Scheme 1. AuNPs/WSe_2/Ti_3C_2 was firstly modified onto CPE. Then SH-FP was immobilized onto it. After the RSV target being added it was amplified with RPA and SA-ALP was attached. 4-APP was catalyzed into 4-AP. The dual redox cycling amplification of TCEP/SQA/4-AP was triggered. This catalytic cycle allowed electrons to be continuously supplied to the solution, thereby resulting in the amplification of the photocurrent response.

As shown in Fig. 6A, the bare CPE exhibited the small semicircle, and the R_{et} value is 250 Ω. After the WSe_2/Ti_3C_2 being drop-cast onto the surface of the CPE, the R_{et} value of the WSe_2/Ti_3C_2/CPE got bigger, indicating that the film formed by the composite material hinders the transfer of electrons to the CPE. But when the WSe_2/Ti_3C_2/CPE was modified with AuNPs, the WSe_2/Ti_3C_2/AuNPs/CPE showed a smaller semicircle and the R_{et} value was about 400 Ω. It is attributed to the excellent conductivity of AuNPs. While SH-DNA, MCH, the products were amplified by RPA and SA-ALP were connected to the WSe_2/Ti_3C_2/

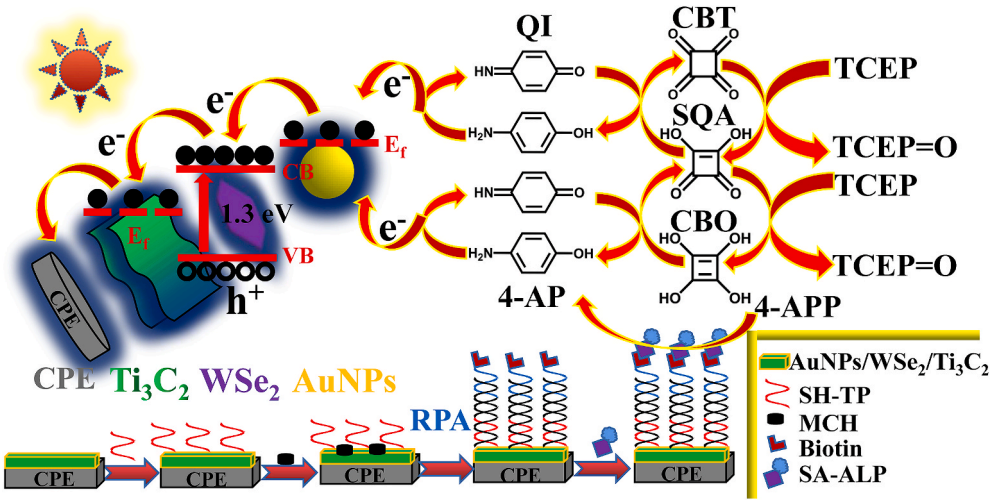

Scheme 1. Schematic experimental procedure for the detection of RSV using RPA and TCEP/SQA/4-AP double redox cycling amplification based on AuNPs/WSe_2/Ti_3C_2 modified electrode.

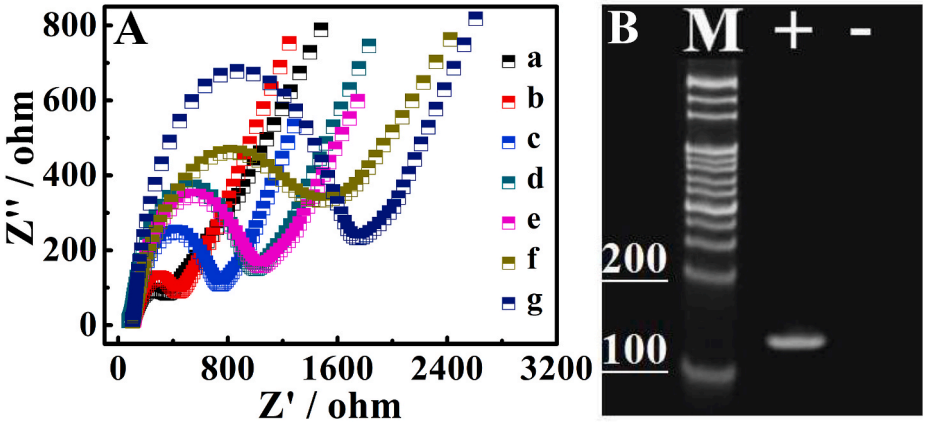

Fig. 6. ESI (A) of (a) CPE, (b) WSe_2/Ti_3C_2/CPE, (c) AuNPs/WSe_2/Ti_3C_2/CPE, (d) SH-RP/AuNPs/WSe_2/Ti_3C_2/CPE, (e) MCH/SH-RP/AuNPs/WSe_2/Ti_3C_2/CPE, (f) Biotin-RP/MCH/SH-RP/AuNPs/WSe_2/Ti_3C_2/CPE, (g) SA-ALP/Biotin-RP/MCH/SH-RP/AuNPs/WSe_2/Ti_3C_2/CPE. (B) PAGE analysis. M, Marker; +, Target; -, Non.

AuNPs/CPE step by step, the relative R_{et} increased correspondingly. This phenomenon indicates that their insulation effect or space effect hinders the electron transfer on the electrode surface. The RPA amplification process was demonstrated by PAGE (Fig. 6B). Lane M is a Mark; Lane-is the product of RPA with each other but without target. When target was introduced into RPA, one band is clearly displayed in Lane + to indicate that successful amplification of RPA. The successful construction of this biosensor is verified by the PEC response (**S4**). The results illustrated that this biosensor was fabricated successfully.

Table 1
Comparison of PEC biosensor and other methods for RSV detection.

Methods	Linear range	LOD	Ref
ColI[a]	0.1–10 pg/mL	0.04 pg/mL	[29]
ELISA	0.5–50 pg/mL	0.5 pg/mL	[30]
PEC	0.2 fM-80 fM	30 aM	This work

[a] ColI: colorimetric immunoassay; ELISA: enzyme-linked immunosorbent assay.

3.6. Analytical performance of PEC biosensor

Under the optimum experimental conditions, the quantitative analysis performance of the PEC biosensor was investigated. Conspicuously, when the RSV concentrations increased, the photocurrent response of the obtained PEC biosensor raised continuously. An ideal linear relationship between the photocurrent response of the biosensor and the logarithm of RSV concentration was obtained. The linear regression equation was I (μA) = 0.7730 log C (fM) + 6.932 (R^2 = 0.9964) with RSV concentration in the range from the 0.2 fM to 80.0 fM (Fig. 7). The comparisons are provided in Table 1. meaning of I, C and R were the photocurrent response, the RSV concentration and the correlation coefficient. LOD was 30 aM. RSD was 3.2% at 1.0 fM.

3.7. Stability, and selectivity of the PEC biosensor

As shown in Fig. 8, the stability of the PEC biosensor was investigated by measuring every six days. And after thirty days storage, the PEC biosensors were monitored. The photocurrent response retains the initial 97.8% that there was not changed obviously. Hence, the PEC biosensor exhibited excellent stability. As for repeatability RSD of PEC response is 3.52% for five consecutive cycles.

The selectivity of the PEC biosensor was monitored by testing several interfering substances, including influenza virus types A (Flu-A), adenovirus (ADV), human rhinovirus (HRV) and human metapneumovirus (HMPV). The blank test photocurrent response demonstrated that there had no difference in comparison with interfering substances (Fig. 8C). While RSV was tested as the detection sample, a dramatically raised photocurrent response was recorded. In addition, when those interfering substances were mixed with RSV, the result that exhibited no significant variation (98.7 ± 2.3%) in the photocurrent response compared with that of RSV alone. It illustrated that this biosensor showed an excellent selectivity towards RSV assay.

3.8. Detection of RSV in practical samples

The feasibility of clinical detection of this sensor was investigated by the method of adding standard recovery. Collect throat secretions of

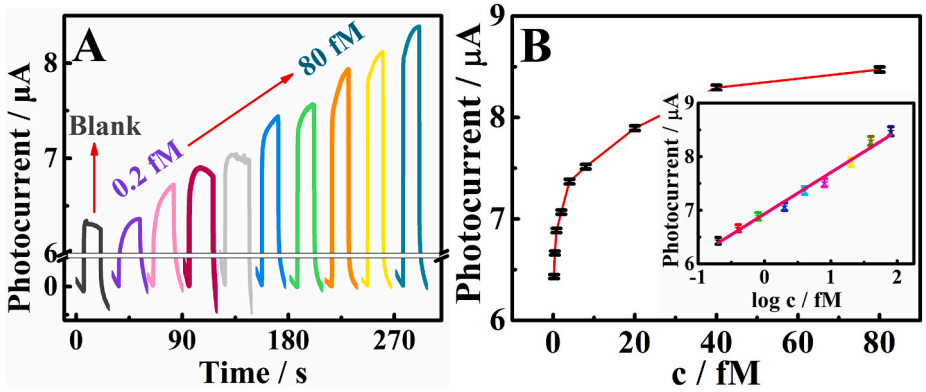

Fig. 7. Calibration plot between photocurrent signals and concentrations of RSV in the concentration range of 0.2 fM-80.0 fM (**A**, **B**). The data points were averaged from eleven electrodes (n = 1).

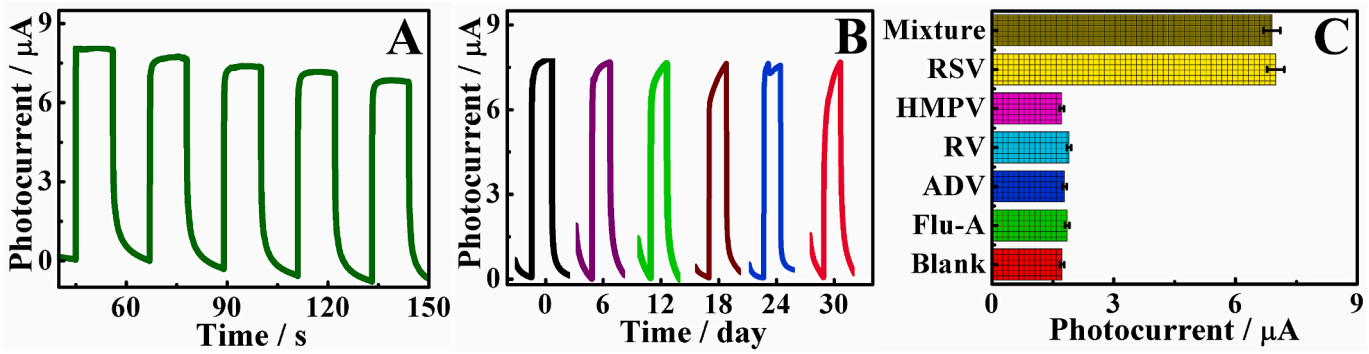

Fig. 8. Stability, repeatability, and interference studies of PEC sensor towards RSV detection. The content of RSV being 80.0 fM.

healthy people, and add RSV with concentrations of 1 fM, 3 fM, 5 fM and 7 fM to the secretions. The sensor constructed as described above was used as the working electrode for testing. The experimental results were shown in Table S1. The recoveries are between 95.8 and 105.0%. The standard method qRT-PCR [31] was also used for comparison. It shows that results of this method are in good agreement with those obtained by qRT-PCR. It indicated the method had good precision and excellent clinical application potential.

4. Conclusion

A photoelectrochemical biosensor based on double redox cycle amplification technology combined with RPA amplification technology was developed here. Firstly, the combination of titanium carbide and tungsten diselenide yields an excellent photosensitive material that can effectively prevent electron-hole pairs from forming fast recombination. Secondly, a new method of effective charge separation through TCEP/SQA/4-AP double redox cycle is proposed. The rapid and efficient feature of RPA isothermal amplification technology is also used to achieve rapid and highly sensitive RSV virus detection. The sensor is inexpensive, easy to operate, has wide applicability, and has development potential, providing a new method for the detection of other biomolecules.

CRediT authorship contribution statement

Xiaohua Li: Conceptualization, Methodology, Resources, Visualization, Validation, Writing – review & editing, Funding acquisition. **Ruhao Wang:** Investigation, Conceptualization, Methodology, Writing – original draft, Writing – review & editing. **Lizhen Liu:** Validation, Writing – review & editing, Methodology, Resources, Visualization. **Xu Hun:** Supervision, Conceptualization, Project administration, Funding acquisition, Resources, Data curation.

Declaration of competing interest

The authors declare that they have no known competing financial interests or personal relationships that could have appeared to influence the work reported in this paper.

Acknowledgments

We thank the support of Entrepreneurship Training Program for College Students (XDC2021203), National Natural Science Foundation of China (NSFC) (21575073) and Laoshan Scholar Program of Qingdao Univ Sci & Technol (201802685).

Appendix A. Supplementary data

Supplementary data to this article can be found online at https://doi.org/10.1016/j.aca.2022.339961.

References

[1] G.Y. Gou, M.L. Jin, B.J. Lee, H. Tian, F. Wu, Y.T. Li, Z.Y. Ju, J.M. Jian, X.S. Geng, J. Ren, Y. Wei, G.Y. Jiang, Y. Qiao, X. Li, S.J. Kim, M. Gao, H.T. Jung, C.W. Ahn, Y. Yang, T.L. Ren, ACS Nano 13 (2019) 12613.
[2] U. Amara, M.T. Mehran, B. Sarfaraz, K. Mahmood, A. Hayat, M. Nasir, S. Riaz, M. H. Nawaz, Microchim. Acta 188 (2021) 230.
[3] K. Huang, C. Li, H. Li, G. Ren, L. Wang, W. Wang, X. Meng, ACS Appl. Nano Mater. 3 (2020) 9581.
[4] H. Dong, L. Cao, Z. Tan, Q. Liu, J. Zhou, P. Zhao, P. Wang, Y. Li, W. Ma, Y. Dong, ACS Appl. Bio Mater. 3 (2020) 377.
[5] Y. Wang, Y. Yue, F. Cheng, Y. Cheng, B. Ge, N. Liu, Y. Gao, ACS Nano 16 (2022) 1734–1758.
[6] W.T. Hsu, L.S. Lu, D. Wang, J.K. Huang, M.Y. Li, T.R. Chang, Y.C. Chou, Z.Y. Juang, H.T. Jeng, L.J. Li, W.H. Chang, Nat. Commun. 8 (2017) 929.
[7] W.W. Zhao, J.J. Xu, H.Y. Chen, Anal. Chem. 90 (2018) 615.
[8] J. Ding, L. Gao, L. Cao, Y. Zhou, H. Wang, J. Duan, H. Yin, J. Sun, S. Ai, Sensor. Actuator. B Chem. 355 (2022), 131290.
[9] X. Hun, Y. Meng, Anal. Chem. 92 (2020) 11771.
[10] N. Hao, Z. Dai, M. Xiong, X. Han, Y. Zuo, J. Qian, K. Wang, Anal. Chem. 93 (2021) 8393.
[11] H. Yin, H. Wu, Y. Chen, F. Li, J. Wang, S. Ai, Microchim. Acta 186 (2019) 663.
[12] X. Fu, R. Huang, J. Wang, X. Feng, Anal. Methods 5 (2013) 3803.
[13] W. Lai, D. Tang, L. Fu, X. Que, J. Zhuang, G. Chen, Chem. Commun. 49 (2013) 4761.
[14] P.A. Jorquera, R.A. Tripp, Expet Rev. Respir. Med. 11 (2017) 609.
[15] Y.Z. Xu, D.Z. Fang, F.F. Chen, Q.F. Zhao, C.M. Cai, M.G. Cheng, Mol. Cell. Probes 49 (2020), 101473.
[16] X. Xu, B. Sun, Z. Liang, H. Cui, J. Tian, ACS Appl. Mater. Interfaces 12 (2020), 26060.
[17] J.S. Nah, S.C. Barman, M.A. Zahed, M. Sharifuzzaman, H. Yoon, C. Park, S. Yoon, S. Zhang, J.Y. Park, Sensor. Actuator. B Chem. 329 (2021), 129206.
[18] W.Y. Chen, X. Jiang, S.N. Lai, D. Peroulis, L. Stanciu, Nat. Commun. 11 (2020) 1302.
[19] W. Feng, H. Luo, Y. Wang, S. Zeng, Y. Tan, L. Deng, X. Zhou, H. Zhang, S. Peng, Sci. Rep. 9 (2019) 3957.
[20] N. Li, Y. Jiang, C. Zhou, Y. Xiao, B. Meng, Z. Wang, D. Huang, C. Xing, Z. Peng, ACS Appl. Mater. Interfaces 11 (2019) 38116.
[21] P. Pataniya, C.K. Zankat, M. Tannarana, C.K. Sumesh, S. Narayan, G.K. Solanki, K. D. Patel, V.M. Pathak, P.K. Jha, ACS Appl. Nano Mater. 2 (2019) 2758.
[22] S. Kumar, M.A. Rehman, S. Lee, M. Kim, H. Hong, J.-Y. Park, Y. Seo, Sci. Rep. 11 (2021) 649.
[23] B. Wang, Y.T. Xu, J.L. Lv, T.Y. Xue, S.W. Ren, J.T. Cao, Y.M. Liu, W.W. Zhao, Anal. Chem. 91 (2019) 3768.
[24] J. Sun, L. An, G. Xue, X. Li, Nanotechnology 31 (2020) 215408.
[25] H.H. Ma, X.B. Zhang, X.Y. Wei, J.M. Cao, Acta Physica Sinica -Chinese Edition 69 (2020), 117101.
[26] Y. Lee, S.B. Cho, Y.C. Chung, ACS Appl. Mater. Interfaces 6 (2014) 14724.
[27] C. Xu, F. Yang, B. Deng, Y. Zhuang, D. Li, B. Liu, W. Yang, Y. Li, J. Catal. 383 (2020) 1.
[28] H. Fang, Y. Pan, M. Yin, L. Xu, Y. Zhu, C. Pan, J. Solid State Chem. 280 (2019) 120981.
[29] L. Zhan, C.M. Li, W.B. Wu, C.Z. Huang, Chem. Commun. 50 (2014) 11526.
[30] L. Zhan, W.B. Wu, X.X. Yang, C.Z. Huang, New J. Chem. 38 (2014) 2935.
[31] J. Hu, M.H. Liu, C.Y. Zhang, Chem. Sci. 9 (2018) 4258.